https://doi.org/10.5194/egusphere-2024-3706
Preprint. Discussion started: 9 December 2024

Nitrate reduction in groundwater as an overlooked source of agricultural CO_2 emissions

Hyojin Kim[1]*, Julian Koch[2], Birgitte Hansen[1] and Rasmus Jakobsen[1]

[1]Department of Geochemistry, Geological Survey of Denmark and Greenland, Øster Voldgade 10. 1350 Copenhagen, Denmark.
[2]Department of Hydrology, Geological Survey of Denmark and Greenland, Øster Voldgade 10. 1350 Copenhagen, Denmark

* Corresponding author: Hyojin Kim (hk@geus.dk)

Abstract

Nitrate pollution from agriculture poses a global environmental and public health threat. Nitrate levels in water can be reduced through denitrification, which increases dissolved inorganic carbon (DIC) via organic carbon mineralization and/or carbonate dissolution. This DIC potentially acts as a net anthropogenic source to atmospheric CO_2; however, its overall impact remains unclear. This study quantified CO_2 production from denitrification in Denmark, utilizing extensive observational datasets and national-scale modelling tools. We identified dominant denitrification processes in groundwater and predicted a national process map. Our results indicate that hydrogeology plays a central role in determining the dominant processes. CO_2 production from denitrification in groundwater varied spatially, depending on nitrogen leaching and the denitrification processes. We estimated that denitrification in groundwater produces about 204 kt of CO_2-eq. yr^{-1} as DIC, and ~50% would be emitted to atmosphere. The Intergovernmental Panel on Climate Change (IPCC) guidelines account CO_2 emissions related to agriculture from liming, urea, and other C-containing fertilizers, and these were 250, 1 and 4 kt of CO_2-eq. yr^{-1}, respectively, for Denmark in 2020. Although CO_2 is a minor agricultural GHG emission (2% of the total), our findings suggest that the agricultural GHG inventories should include denitrification-related CO_2 emissions.

1. Introduction

The application of nitrogen (N) inorganic fertilizers and animal manure in agriculture is essential for global food production. However, their use poses significant environmental and public health risks (Diaz and Rosenberg, 2008; Galloway et al., 2003; Howarth et al., 2011; Jensen et al., 2023; Schullehner et al., 2018; Temkin et al., 2019; Trends et al., 2008; Ward et al., 2018). Reactive N, primarily in the form of nitrate (NO_3^-), leaches from agricultural soils into nearby aquatic ecosystems, leading to eutrophication and hypoxic "dead zones" in coastal areas (Diaz and Rosenberg, 2008; Galloway et al., 2003; Howarth et al., 2011). Elevated nitrate concentrations in drinking water are associated with several health risks, such as infant methemoglobinemia (blue baby syndrome). The current regulatory limit for nitrate in drinking water (50 mg/L as

https://doi.org/10.5194/egusphere-2024-3706
Preprint. Discussion started: 9 December 2024

nitrate) is set to prevent this condition, yet recent studies have shown that the risks of certain cancers and birth defects may increase at concentrations below this threshold (Jensen et al., 2023; Schullehner et al., 2018; Temkin et al., 2019; Ward et al., 2018).

Nitrogen fertilizers are also a major source of anthropogenic greenhouse gases (GHGs; Gao and Cabrera Serrenho, 2023; Menegat et al., 2022; Mosier et al., 1998; Zamanian et al., 2018). Nitrate undergoes denitrification, a sequence of redox reactions that converts it to nitrite (NO_2^-), nitrogen monoxide (NO), nitrous oxide (N_2O) and finally inert nitrogen (N_2) gas. Nitrous oxide is a potent GHG, with 265 times the warming potential of carbon dioxide (CO_2). Nearly all global N_2O emissions originate from agricultural fertilizer applications (Ritchie et al., 2023), primarily from soils, while 10-15 % occurs via indirect pathways such as groundwater, streams, and estuaries (Gao and Cabrera Serrenho, 2023; Nielsen et al., 2022). The use of N-fertilizers also contributes to soil acidification through microbial oxidation of ammoniacal fertilizer or urea application (Barak et al., 1997):

(nitrification of ammonia): $NH_3 + 2O_2 = H^+ + NO_3^- + H_2O$
(nitrification of ammonium): $NH_4NO_3 + 2O_2 = 2H^+ + 2NO_3^- + H_2O$
(hydrolysis of urea and nitrification of products): $CO(NH_2)_2 + 4O_2 = 2H^+ + 2NO_3^- + CO_2$

Liming is commonly used to counteract acidification, but both liming and urea applications lead to CO_2 emissions (Zamanian et al., 2018). In terms of CO_2 equivalents (CO_2-eq.), liming is comparable to the indirect N_2O emissions (Gao and Cabrera Serrenho, 2023; Zamanian et al., 2018) while CO_2 from urea is relatively insignificant (Nielsen et al., 2022).

During denitrification, another greenhouse gas, CO_2, is also produced. When oxygen is completely depleted and reduced materials (electron donors) such as organic matter are available, nitrate can be reduced to N_2 gas, simultaneously increasing dissolved inorganic carbon (DIC) in water (Equation 1 in Table 1; Appelo and Postma, 2005; Seitzinger et al., 2006). This process mineralizes organic carbon (shown as CH_2O), releasing 5 moles of DIC per 4 moles of N reduction. Pyrite can be oxidized by oxygen (Equation 3 in Table 1) as well as nitrate (Equation 2 in Table 1; Postma et al., 2012; Torrentó et al., 2010; Zhang et al., 2009). Both reactions (2 and 3) produce protons that can dissolve carbonate minerals if present (Equation 5 in Table 1).

https://doi.org/10.5194/egusphere-2024-3706
Preprint. Discussion started: 9 December 2024

Table 1. Reactions considered in this study and key stoichiometric ratios of the reactions.

	Groundwater chemistry			CO_2 emissions per mole of N reduced $(\frac{+\Delta CO_2}{-\Delta NO_3^-})^{**}$
	$\frac{HCO_3^-}{Ca^{2+}+Mg^{2+}}$	$\frac{SO_4^{2-}}{Ca^{2+}+Mg^{2+}}$	$\frac{+\Delta DIC}{-\Delta NO_3^-}$	
Denitrification reactions				
(1) Denitrification with organic C oxidation: $5CH_2O + 4NO_3^- \rightarrow 2N_2 + 4HCO_3^- + H_2CO_3 + 2H_2O$	>2	-	1.25	0.625
(2) Complete denitrification with pyrite oxidation 2a) $5FeS_2 + 14NO_3^- + 4H^+ \rightarrow 7N_2 + 5Fe^{2+} + 10SO_4^{2-} + 2H_2O$ 2b) $5Fe^{2+} + NO_3^- + 12H_2O \rightarrow 0.5N_2 + 5Fe(OH)_3 + 9H^+$ $= 5FeS_2 + 15NO_3^- + 10H_2O \rightarrow 7.5N_2 + 5Fe(OH)_3 + 10SO_4^{2-} + 5H^+$	1*	2*	0.33*	0.17*
Other reactions				
(3) Pyrite oxidation with oxygen $FeS_2 + {}^{15}/_4\, O_2 + {}^{7}/_2\, H_2O \rightarrow Fe(OH)_3 + 2SO_4^{2-} + 4H^+$	1*	0.5*	-	-
(4) Reversible reaction of carbonate dissolution with CO_2 and carbonate precipitation $xCa^{2+} + (1-x)\, Mg^{2+} + 2HCO_3^- \leftrightarrow Ca_xMg_{(1-x)}CO_3(s) + CO_2(g) + H_2O$	2	-	-	-
(5) Carbonate dissolution with strong acids $5Ca_xMg_{(1-x)}CO_3 + 5H^+ \rightarrow 5xCa^{2+} + 5(1-x)\, Mg^{2+} + 5HCO_3^-$				

*Coupled with carbonate dissolution; ** In case of calcite saturation

These processes elevate DIC levels in streams and groundwater, which naturally have significantly higher partial pressure of CO_2 (pCO_2) than the atmosphere, largely due to soil respiration, resulting in CO_2 emissions from these waters (Duvert et al., 2018; Macpherson, 2009; Martinsen et al., 2024). If groundwater or stream water reaches the saturation point of calcite as CO_2 degasses, calcite will precipitate (Equation 4 in Table 1). In this case, while one mole of DIC is re-stored as calcite, the other is release as CO_2. This series of processes i.e., from denitrification to calcite precipitation do not involve atmospheric

https://doi.org/10.5194/egusphere-2024-3706
Preprint. Discussion started: 9 December 2024

CO_2 and are triggered by anthropogenic nitrate input from agriculture, making them a net anthropogenic source of atmospheric CO_2.

Globally, approximately 50 teragrams (Tg; 10^{12} g) of N are lost from agricultural soils annually through leaching and erosion (Liu et al., 2010), and the subsurface serves as a large reservoir of reactive N (Ascott et al., 2017). Denitrification of this leached N below the soil layer could represent a significant indirect pathway for agriculturally derived CO_2 emissions. Unlike nitrate in streams and/or estuaries which could promote primary productivity, thus fixing CO_2; nitrate in groundwater is simply a pollutant and a potential source of CO_2 when it is reduced. Furthermore compared to direct emissions from soil, which occur promptly, indirect pathways via groundwater exhibit dispersed and delayed signals due to long and variable transit times (Basu et al., 2022; Meals et al., 2010). This delay could potentially undermine the effectiveness of climate mitigation efforts and increase uncertainty of GHG inventories and future projections.

Despite its potential importance, CO_2 emissions due to denitrification, especially from groundwater, have not been investigated. According to the Intergovernmental Panel on Climate Change (IPCC) guidelines, anthropogenic GHG emissions from managed soils—*land where human interventions and practices have been applied to perform production, ecological or social functions* (IPCC, 2006)—include 1) direct (i.e., soil) and indirect (i.e., stream, groundwater, and estuary) N_2O emissions from N fertilizer input; and 2) direct (i.e., soil) CO_2 emissions from liming, urea and other CO_2-containing fertilizers. The guidelines do not account for CO_2 emissions from or derived from denitrification (IPCC, 2006).

This study, therefore, aims to quantify the magnitude of CO_2 released from denitrification associated with agricultural N-fertilizer use in the context of national GHG inventories. In Denmark, a national groundwater monitoring program provides extensive long-term data of groundwater chemistry across the country (Thorling et al., 2024). Additionally, the National Nitrogen Model (den Nationale KvælstofModel; NKM) provides a national N budget at the catchment scale (Højberg et al., 2021). These data and tools effectively transform Denmark into a virtual laboratory for quantitative and systematic investigations of CO_2 emissions resulting from denitrification of nitrate derived from N-fertilizer at a national scale. Using these resources, along with machine learning techniques, we addressed three specific objectives: 1) characterization of geochemical architecture of Danish groundwater, focusing on redox conditions and dominant denitrification processes; 2) prediction of a national map of denitrification processes; and 3) quantification of the contribution of CO_2 from denitrification in the agriculture GHG inventory at the national scale.

2. Method and materials

2.1. Groundwater chemistry data

Groundwater chemistry data were retrieved from the National Borehole Database, Jupiter (www.geus.dk) in November 2022. The dataset includes all the groundwater chemistry data deposited in Jupiter in the period 1890-2022. A total of

https://doi.org/10.5194/egusphere-2024-3706
Preprint. Discussion started: 9 December 2024

186,887 records from 36,216 screens across the country were extracted. To ensure the data quality and integrity, the dataset was cleaned using five exclusion criteria: 1) wells within a 100 m buffer zone of landfill sites; 2) wells identified as contaminated with micro-organic pollutants by the Danish Environmental Protection Agency; 3) records with incomplete geographical information (x, y, and screen depth); 4) duplicate entries; and 5) records with detection limits exceeding 1 mg/L for NO_3^-, SO_4^{2-}, Ca^{2+}, Mg^{2+}, and HCO_3^-, which indicate low analytical quality. Post-cleaning, the dataset contained 115,276 records from 24,323 screens.

Approximately 70% of these screens were sampled only once, with varying combinations of solutes measured. For further analysis, we selected screens that 1) had at least five measurements of NO_3^-, SO_4^{2-}, HCO_3^-, Ca^{2+}, and Mg^{2+} over the entire period; and 2) had at least one measurement for pH, Fe^{2+}, Mn^{2+}, CH_4, NH_4^+, Na^+, and Cl^-. This process resulted in 6,273 screens being included in the final dataset. Finally, values below detection limits were converted to half of the detection limit.

2.2. Characterization of geochemical architecture of the Danish groundwater

The cleaned dataset was analyzed to categorize redox conditions and to identify dominant processes by combining two machine learning techniques: Non-negative Matrix Factorization (NMF) and K-means clustering. The analyses were done in MATLAB using built-in functions. Both methods are widely used for identifying sources and underlying processes of water chemistry (Haggerty et al., 2023; Kim et al., 2021; Shaughnessy et al., 2021; Vesselinov et al., 2018). Specifically, the results of NMF can be interpreted as endmembers and their mixing ratios (Haggerty et al., 2023; Shaughnessy et al., 2021; Vesselinov et al., 2018), which we used as a pre-processing step before applying K-means clustering. Since groundwater chemistry can be influenced by mixing and/or result from a series of processes, this approach reduced data dimensionality and enhanced the robustness of the subsequent clustering.

NMF decomposes the original matrix (V) into two non-negative matrices: one representing endmember compositions (H) and the other representing contributions (i.e., mixing proportion; W) of these endmembers in the context of hydrogeochemistry:

$$V = H \times W$$

The optimal number of endmembers was determined using the Elbow method, which is commonly used in clustering analysis to find the optimal number of clusters by plotting the sum of squared error (SSE) as a function of clusters (Syakur et al., 2018). In our study, the optimal endmember number of endmembers was identified at the minimum reconstruction error. The mixing ratios (matrix W) were subsequently used for K-means clustering. The Silhouette score—a measure of how well each data point fits within its own cluster while remaining well-separated from others—and within-cluster sum of square (WCSS) —a measure of the variability within each cluster—were used to determine the optimal cluster number. K-means clustering was repeated 50 times to achieve the highest silhouette score and the lowest WCSS.

https://doi.org/10.5194/egusphere-2024-3706
Preprint. Discussion started: 9 December 2024

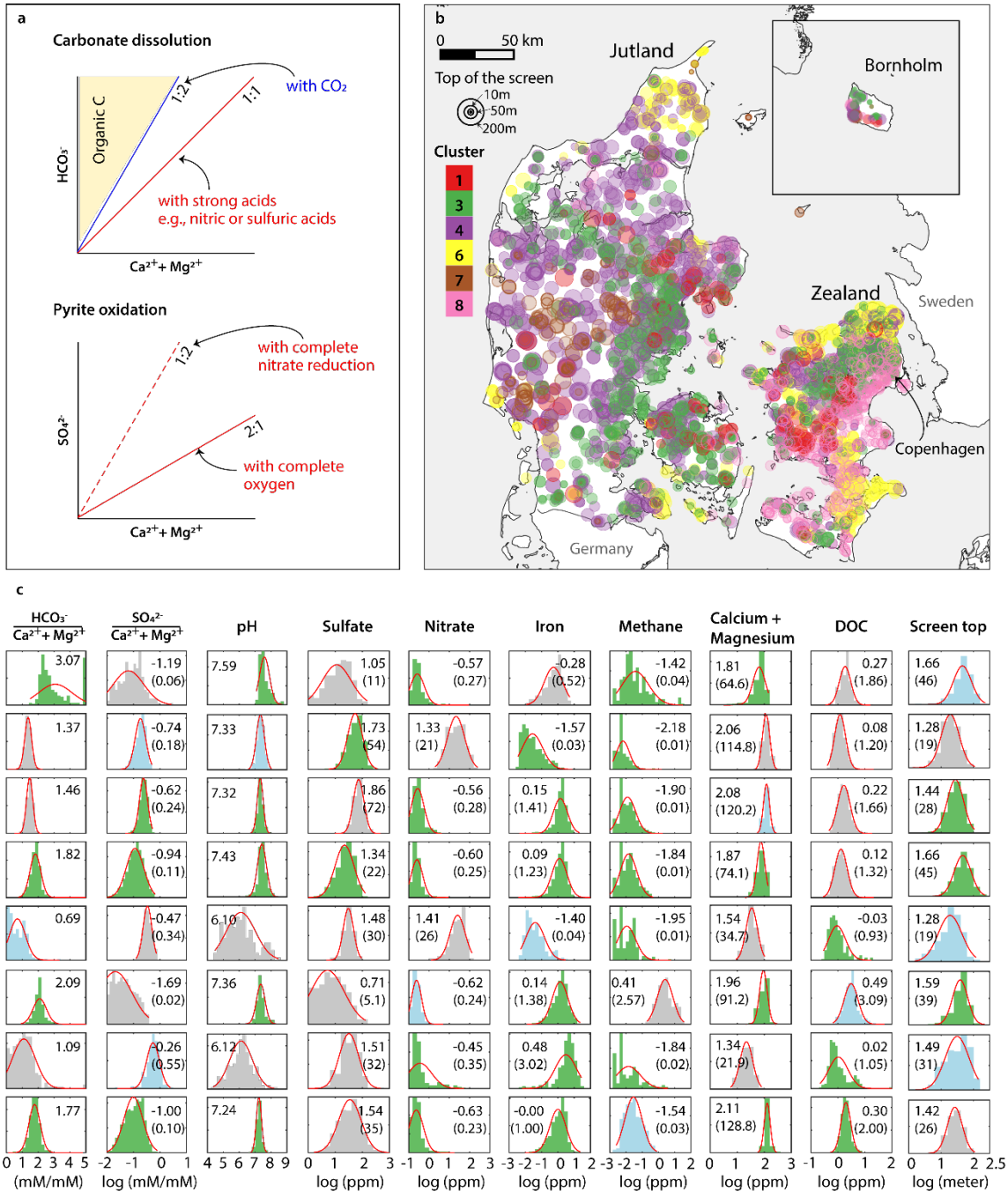

Figure 1: Overview of the groundwater chemistry analysis results. a. Theoretical relationships of Ca^{2+} + Mg^{2+} vs. HCO_3^- and vs. SO_4^{2-} for key processes of the study. b. Map of cluster distribution. Marker colors represent different clusters, and marker sizes indicate the depth to the top of the screen. The oxic clusters (cluster 2 and 5) are not shown (available in Supplementary Figure s1). c. Histograms of the Non-negative Matrix Factorization (NMF) and K-means clustering results for groundwater. The red lines represent the probability distribution function of a normal distribution. The green, blue, and gray bars correspond to p-values <0.01, 0.01-0.05, and >0.05, respectively. The values displayed in the histograms are means (μ), and the numbers in parentheses are back-transformed values.

https://doi.org/10.5194/egusphere-2024-3706
Preprint. Discussion started: 9 December 2024

To further supervise the NMF and clustering analysis, we computed the mean stoichiometric ratios of $\frac{HCO_3^-}{(Ca^{2+}+Mg^{2+})}$ and $\frac{SO_4^{2-}}{(Ca^{2+}+Mg^{2+})}$ at the screen level. To minimize the impact of outliers, the stoichiometric ratios were calculated by randomly selecting 70% of the data for each screen and calculating the mean ratios 20 times. Outliers from these subsets were excluded from the final mean ratio calculations for each screen. These two ratios can provide insights into the dominant denitrification processes and the source of DIC. When carbonate dissolution occurs due to CO_2 derived carbonic acid, the $\frac{HCO_3^-}{Ca^{2+}+Mg^{2+}}$ ratio equals 2, with no effect on SO_4^{2-} concentrations (Figure 1a; Equation 4 Table 1). If carbonate dissolution is coupled with pyrite oxidation, the $\frac{HCO_3^-}{Ca^{2+}+Mg^{2+}}$ ratio becomes 1, and its $\frac{SO_4^{2-}}{Ca^{2+}+Mg^{2+}}$ ratio will be either 2 (with nitrate, Equation 2 + 5 in Table 1; Figure 1a) or 0.5 (with oxygen, Equation 3 +5 in Table 1; Figure 1a). When organic carbon mineralization occurs without carbonate minerals, HCO_3^- concentrations increase without changing Ca^{2+} and Mg^{2+} concentrations, resulting in a $\frac{HCO_3^-}{Ca^{2+}+Mg^{2+}}$ ratio greater than 2 (Figure 1a). Additionally, means of all the available constituents were also calculated at the screen level, and redox sensitive elements such as nitrate, sulfate, iron and methane were included in the anlaysis to interpret the redox conditions of the clusters (All the elements listed in Supplementary Table s1). All values were log-transformed and normalized before analysis.

2.3. Prediction of the national map of denitrification processes at the redox interface

After identifying the redox conditions and dominant processes in groundwater, this point-scale information was upscaled to predict a national map of denitrification processes at the redox interface. In Denmark, the redox interface i.e., the bottom of nitrate-reducing zone was predicted on the national scale (25m x 25m resolution) based on sediment color data and 20 explanatory variables (Table 2) using a gradient boosting with decision trees (GBDT) algorithm (Koch et al., 2024). By employing the same method and variables, we predicted the national denitrification process map (100 m x 100 m resolution). GBDT is a commonly used machine learning technique in various fields for solving prediction tasks in both classification and regression. Through iterative training, GBDT builds ensemble-based prediction models using weak learners (i.e., decision trees). The ensemble is iteratively improved by adding decision trees that focus on correcting the residuals of the previous model. We used Microsoft's LightGBM (Light Gradient Boosting Machine) implementation of the GBDT algorithm in this study (Ke et al., 2017).

https://doi.org/10.5194/egusphere-2024-3706
Preprint. Discussion started: 9 December 2024

Table 2. Explanatory variables for prediction of denitrification process map

Covariate	Description	Source
Clay a	Clay content (%), 0-30 cm	Adhikari et al. (2013)
Clay b	Clay content (%), 30-60 cm	
Clay c	Clay content (%), 60-100 cm	
Clay d	Clay content (%), 100-200 cm	
DEM	Elevation above sea level (m)	Danish Agency for Data Supply and Infrastructure (SDFI)
Slope	Surface slope gradient (deg)	
Geo-region	Geological regions of Denmark	Adhikari et al. (2014)
Landscape E.	Landscape types of Denmark	Aarhus University - Danish Centre for Environment and Energy
Wetland	Wetland classification (mineral/organic)	
DEM Var.	Deviation between high-resolution and low-resolution elevation (m)	
d. to stream	Horizontal distance to stream network (m)	
Geo. Complex.	Geological complexity	Sandersen (2021)
Clay thick.	Thickness of clay deposits – from surface (m)	National Water Resources model (DK-model)
Sand thick.	Thickness of sand deposits – from surface (m)	
Aquifer thick.	Thickness of uppermost aquifer (m)	
Q. thick	Thickness of Quaternary deposits – from surface (m)	
Mean gwt.	Mean water table depth (m.b.g.l.)	
Max gwt.	Maximum water table depth (m.b.g.l.)	
recharge	Recharge (mm/year)	

For the prediction of the denitrification process map, we first excluded groundwater screens from 1) oxic clusters; and 2) reduced clusters with a Silhouette score less than 0. Among the remaining screens, we selected those located near the redox interface. Considering the uncertainty of the redox interface map (Koch et al., 2024) and the availability of the groundwater chemistry data used for clustering, three subsets of groundwater chemistry data were selected: depths of groundwater screens shallower than the depths of redox interface minus 5 (D5), 10 (D10), and 15 (D15) meters. This resulted in 235 (D5), 566 (D10) and 1019 (D15) wells for training, respectively (Supplementary Figure s1). The three depth derived models were evaluated based on a 2-fold cross validation procedure i.e. training two models, each using 50% of the data for training and validating against the remaining 50%. The model's uncertainty was quantified through bootstrapping, by repeatedly training

https://doi.org/10.5194/egusphere-2024-3706
Preprint. Discussion started: 9 December 2024

the classification model and predicting the denitrification process map. We generated 100 realizations of the process map for each depth criterion, each based on bootstrapped samples (with replacement).

The Shapley additive explanations (SHAP) approach was employed to assess the sensitivity of the trained classification models, i.e., feature importance (Lundberg and Lee, 2017). SHAP, based on game theory principles, explains the output of machine learning models by attributing predictions to individual covariates, quantifying their marginal contributions. In this study, absolute SHAP values were used to measure feature importance. SHAP values are reported for each class, i.e. each cluster in the classification model, and as an average across the classes.

2.4. Estimation of DIC produced by denitrification in groundwater

The DIC production due to denitrification was estimated by combining the predicted process maps with the average of groundwater nitrate reduction estimates from 1990-2010 provided by the National Nitrogen Model (NKM). NKM is a comprehensive model that links three existing models (Henriksen et al., 2003; Højberg et al., 2015, 2017): 1) empirical, statistical models for N leaching from the root zone (NLES; Børgesen et al., 2020); 2) the National Water Resource model (DK-model; Stisen et al., 2019) with particle tracking in MIKE-SHE for groundwater and drain flow and N reduction; and 3) statistical models for N reduction in surface waters such as streams and lakes. Nitrogen reduction is simulated at the catchment level, where the average catchment size is roughly 15 km^2. Nitrogen reduction in groundwater is calculated based on the fraction of particles passing through the redox interface, assuming instantaneous and complete denitrification at the interface. The NKM was developed, calibrated and validated using 21 years of measurements from 340 stream stations, covering approximately half of Denmark.

The groundwater N reduction estimates (kg N ha^{-1} yr^{-1}) at the catchment level, provided in shapefile format, were converted into a GeoTIFF file using QGIS to match the extent and grid size (100m x 100m) of the denitrification process map. For each of the 100 realizations of the process maps, the groundwater N reduction and cluster data were linked at the grid level using MATLAB. DIC production for each grid cell (i) were calculated by multiplying groundwater N reduction (GNRi) and the stoichiometric ratio of DIC production per N reduction for the respective cluster (r_i):

$$DIC\ produced\ by\ denitrification\ (kt\ CO_2\ y^{-1}) = \left[\sum_{i=1}^{n}(GNR_i\ \times\ r_i \times {}^{44}/_{14}\ \times\ 10^3)\right] \times 10^{-9}$$

where r_i values are 1.25 for denitrification by organic carbon and 0.33 for denitrification by pyrite oxidation coupled with carbonate dissolution (Table 1). The estimated DIC production was first summed up for the catchment level and then to the national level. The mean (μ) and standard deviation (σ) of DIC production from the 100 realizations for D5, D10 and D15, respectively, were calculated using MATLAB.

https://doi.org/10.5194/egusphere-2024-3706
Preprint. Discussion started: 9 December 2024

3. Results and Discussion

3.1. Geochemical architecture of the Danish groundwater

Our results demonstrate that the Danish groundwater can be categorized into eight clusters): two oxic clusters (cluster 2 and 5) and six reduced clusters (1, 3, 4, 6, 7, and 8), each at various redox stages (Figure 1c). The mean silhouette score for the clustering results in this study was 0.45. Figure 1c presents histograms of the concentrations and stoichiometric ratios of input parameters. The two oxic clusters were characterized by high nitrate concentrations (mean (μ) = 21 and 26 mg/L, respectively), low iron concentrations (μ = 0.03 and 0.04 mg/L, respectively) and relatively shallow depths (μ = 19 m for both; Figure 1c). These clusters exhibited $\frac{HCO_3^-}{Ca^{2+}+Mg^{2+}}$ ratios of 1.37 (cluster 2) and 0.67 (cluster 5), suggesting a strong influence of anthropogenic impact, such as nitric acid produced by microbial oxidation of ammoniacal fertilizers as mentioned earlier (Barak et al., 1997; Perrin et al., 2008). Cluster 2 was found mainly in the eastern part of Denmark while cluster 5 were mainly in the western and northern regions (Supplementary Figure s2). Denitrification in these oxic clusters was considered negligible; therefore, further interpretations focused on the six reduced clusters.

The six reduced clusters exhibited nitrate concentrations below 1 mg/L and elevated iron concentrations (μ = 0.52-3.02 mg/L; Figure 1c). Cluster 1 and 6 showed high $\frac{HCO_3^-}{Ca^{2+}+Mg^{2+}}$ ratios (μ = 3.07 and 2.09, respectively; Figure 1c), indicating the dominance of organic carbon oxidation. Sulfate concentrations varied widely in both clusters, but the mean values were the lowest among all the reduced clusters (μ =11 and 5 mg/L, respectively; Figure 1c), indicative of sulfate reduction. Notably, cluster 6 exhibited high methane concentrations (μ = 2.57 mg/L; Figure 1c), suggesting highly reduced methanogenic conditions.

Cluster 3 had the highest sulfate concentrations (μ = 72 mg/L) and the second-highest Fe concentrations (μ = 1.41 mg/L; Figure 1c). The elevated sulfate levels were attributed to pyrite oxidation, and its elevated Fe concentration could be due to incomplete pyrite oxidation and/or reductive dissolution of Fe(II)-bearing minerals. While anthropogenic sulfur input can elevate sulfate concentrations in groundwater, cluster 3 displayed higher sulfate concentrations than the oxic clusters (μ = 54 and 30 mg/L, respectively). Since the oxic clusters were generally closer to the direct input of recharge and thus more responsive to anthropogenic signals, we conclude that pyrite oxidation likely plays a larger role in the elevated sulfate concentrations in this cluster. However, the $\frac{SO_4^{2-}}{Ca^{2+}+Mg^{2+}}$ ratios were lower than the theoretical values for pyrite oxidations (μ = 0.24). This discrepancy may arise if carbonate mineral dissolution occurs by both strong (nitric and sulfuric acids) and carbonic acids (H_2CO_3; $\frac{HCO_3^-}{Ca^{2+}+Mg^{2+}}$ = 2) as indicated by the μ of the $\frac{HCO_3^-}{Ca^{2+}+Mg^{2+}}$ ratio of 1.48. This value aligns with ratios typical of agricultural streams (Perrin et al., 2008; Stets et al., 2014), supporting our interpretation.

Cluster 4 was characterized by low sulfate concentrations (μ = 22 mg/L) and found at deeper depths (μ = 45m). These conditions indicated moderately reduced states, likely transitioning from Fe-reducing to sulfate reducing conditions. The high $\frac{HCO_3^-}{Ca^{2+}+Mg^{2+}}$ ratios (μ = 1.82) and relatively low Ca^{2+} + Mg^{2+} concentrations (μ = 74 mg/L) were attributed to HCO_3^-

https://doi.org/10.5194/egusphere-2024-3706
Preprint. Discussion started: 9 December 2024

production from the oxidation of organic carbon by reducing sulfate and Fe-oxides, in groundwater already in equilibrium with carbonate minerals (e.g. calcite).

Cluster 7 showed the highest Fe concentrations (μ = 3.02 mg/L) and lowest pH (μ = 6.12) among the reduced clusters (Figure 1c). Its mean $\frac{SO_4^{2-}}{Ca^{2+}+Mg^{2+}}$ and $\frac{HCO_3^-}{Ca^{2+}+Mg^{2+}}$ ratios were 0.55 and 1.09, respectively, closely aligning with those of pyrite oxidation with oxygen coupled with carbonate dissolution (Equation 3 and 5 in Table 1). Previous transect-level studies from the area near cluster 7 documented that denitrification in groundwater is mediated by pyrite oxidation (Jessen et al., 2017; Postma et al., 1991). They also reported that the study area is depleted with carbonates and attributed total inorganic carbon (TIC) in groundwater to agricultural liming. The low pH and Ca^{2+} + Mg^{2+} concentrations of cluster 7 are consistent of these studies' results. However, cluster 7 displayed low sulfate (μ = 32 mg/L) but high Fe (μ = 3.02 mg/L) concentrations for conditions dominated by complete denitrification by pyrite oxidation (Equation 2 in Table 1). For instance, Danish oxic groundwater displays between 40-50 mg/L of nitrate (Thorling et al., 2024). If it is denitrified by pyrite oxidation, it will result an increase of SO_4^{2-} concentrations by 41-51 mg/L and very low Fe concentrations. We attributed these discrepancies to either/or combinations of 1) sulfate and iron reduction by oxidation of organic carbon; 2) mixing with reduced groundwater from deeper depths; and/or 3) incomplete oxidation of S^{-1} of pyrite (Zhang et al., 2009):

$$20FeS_2 + 14NO_3^- + 44H^+ \rightarrow 20\,Fe^{2+} + 5SO_4^{2-} + 35S^0 + 7N_2 + 22H_2O$$

The low $\frac{HCO_3^-}{Ca^{2+}+Mg^{2+}}$ ratios of cluster 7 imply that a role of organic carbon decomposition may be minor; thus, the second and/or third processes may be more likely responsible for the cluster 7 groundwater chemistry.

Cluster 8 exhibited signs of transitioning from Fe- to sulfate-reducing/methanogenic environments in organic- and carbonate-rich conditions. The $\frac{HCO_3^-}{Ca^{2+}+Mg^{2+}}$ ratio (μ = 1.7) was significantly higher than for carbonate dissolution by strong acids. Moderately elevated dissolved organic carbon (DOC; μ= 2.0 mg/L) and detectable methane (μ= 0.03 mg/L) indicated an abundance of organic C. Additionally, this cluster exhibited the highest Ca^{2+} + Mg^{2+} concentrations among all clusters, further supporting carbonate-rich conditions.

Altogether, we hypothesized that if cluster 3 and 7 are found around the redox interface, denitrification in these regions will likely be mediated by pyrite oxidation. Both clusters displayed pyrite oxidation signals and completion of nitrate reduction, which are expected at the bottom of the redox interface. Conversely, if cluster 1 and 6, representing highly reduced conditions, are found at the redox interface, denitrification in these areas may be mediated by organic carbon oxidation. These clusters are expected to appear in areas with abundant highly reactive organic matter, where the thicknesses of nitrate-reducing and iron-reducing zones may be too thin to resolve at the scale of most of the groundwater screens. Cluster 4 and 8, interpreted as transitioning to Fe- and sulfate reducing/methanogenic conditions, did not display clear dominance of either pyrite oxidation or organic C oxidation. However, we suggest that organic C oxidation may be more dominant in these clusters as indicated by their $\frac{HCO_3^-}{Ca^{2+}+Mg^{2+}}$ ratios compared to those of pyrite oxidation cases.

https://doi.org/10.5194/egusphere-2024-3706
Preprint. Discussion started: 9 December 2024

3.2. A national map of denitrification processes at the redox interface

Figure 2a shows the predicted spatial distribution of clusters at the redox interface with the distance criterion of 10 m (D10). Results for D5 (5 m) and D15 (15m) are available in Supplementary Figures s1. The overall accuracies based on the 2-fold cross validation were 0.58 (D5), 0.61 (D10), and 0.64 (D15), respectively. The final maps (Figure 2a and Supplementary Figure s1) of denitrification processes were generated by GBDT models trained against 100% of the available data.

The denitrification process map resembles the landscape elements of Denmark (Figure 2c), although its feature importance was close to zero except for cluster 7 (Figure 2b). Among the 20 explanatory variables, the thickness of Quaternary deposits and groundwater recharge were identified as the two most influential variables (Figure 2b). These findings highlight the central role of hydrogeology in determining the distribution of clusters at the redox interface. For instance, cluster 7, representing nitrate-reduction by pyrite oxidation in carbonate-limited environments, was predicted predominantly in meltwater plain areas outside the main stationary line of the ice sheet of the last glaciation. In contrast, cluster 3, interpreted similarly but under carbonate-rich conditions, was mainly found behind the main stationary line. This difference likely arises because the meltwater plains beyond the main stationary line have been exposed to weathering for longer than areas covered by ice sheets, leading to the depletion of easily weatherable minerals such as carbonates. Additionally, groundwater recharge emerged as the most influential predictive variable for cluster 7, further suggesting intensive weathering. Overall, cluster 7 corresponds to more intensively weathered hydrogeological conditions.

In the postglacial (more recent) sediment areas, where fresh organic matter is likely abundant, highly reduced conditions were predicted around the redox interface, which is consistent with our hypothesis of the cluster distribution at the redox interface. Cluster 6, associated with methanogenesis, would require extremely reactive organic matter, which is consistent with its presence in dunes and postglacial marine sediment areas (Hansen et al., 2001; Jakobsen and Cold, 2007; Jakobsen and Postma, 1999). The thickness of the Quaternary deposits and the mean depth of the groundwater table were the most important predictors for cluster 6, implying that the combination of organic-rich and a shallow groundwater table can result in such extremely reduced conditions. Cluster 1 (sulfate reducing conditions) rarely appeared near the redox interface.

https://doi.org/10.5194/egusphere-2024-3706
Preprint. Discussion started: 9 December 2024

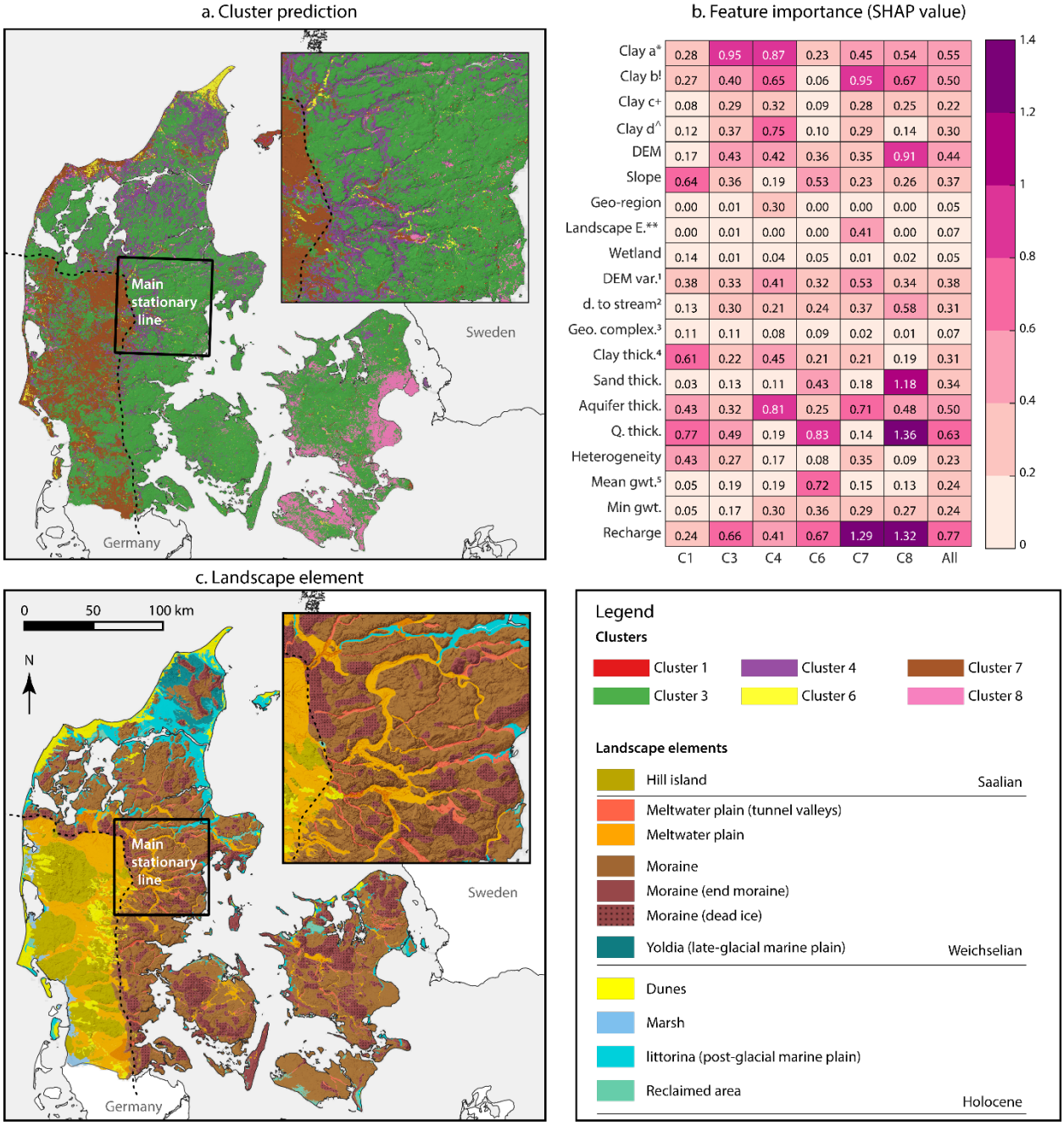

Figure 2. a. Map of denitrification processes at the redox interface with the distance criterion 10 m from the redox interface to the screen tops (D10). b. Feature importance of the 20 input variables used for map prediction. *Clay a: clay content (%) 0-30 cm; [!]Clay b: Clay content (%) 30-60 cm; [+]Clay c: clay content (%) 60-100 cm; ^Clay d: clay content (%), 100-200 cm;Landscape E.: Landscape Element; [1]DEM var.: Digital Elevation Map variability; [2]d. to stream: horizontal distance to stream network (m); [3]Geo. Complex.: geological complexity; [4]Clay thick.: thickness of clay deposits from the surface (m). Sand thick., Aquifer thick., and Q. thick. refer to the thickness of sandy layer, aquifer, and quaternary layers, respectively; [5]Mean gwt.: mean depth to groundwater table in meters below the ground level. c. Landscape element map of Denmark with the legend displayed on the right.**

https://doi.org/10.5194/egusphere-2024-3706
Preprint. Discussion started: 9 December 2024

The spatial distributions of cluster 4 and cluster 8, which transition from Fe- to sulfate-reducing conditions, were also distinctive. Cluster 4 was mostly found in postglacial marine sediments and meltwater plains within the main stationary line. These meltwater plains typically evolve into river valleys (Kaiser et al., 2007), where recent reactive organic matter accumulates. While cluster 8 was predicted in areas where a thin Quaternary layer overlays limestone in Zealand. This limestone is primarily the Danian bryozoan limestone, formed in cool and deep-water conditions shortly after the Cretaceous-Tertiary (K/T) mass extinction (Bjerager and Surlyk, 2007; Jorgensen, 1988). The limestone represents a highly diverse marine benthic ecosystem, rich in organic matter such as bryozoan-coral mounds (Bjerager and Surlyk, 2007; Jorgensen, 1988), leading to formation of pyrite in the limestone from sea water sulfate. Indeed, in bryozoan limestone, pyrite is observed (Damholt et al., 2006). In both cluster 4 and 8, pyrite oxidation may be probable. However, the groundwater chemical signatures (i.e., $\frac{HCO_3^-}{Ca^{2+}+Mg^{2+}}$ ratios and highly reduced conditions) of these two clusters may indicate a more dominant role of organic C oxidation.

3.3. Anthropogenic DIC production in groundwater due to N fertilizer applications

For the period 1990-2010, the NKM estimated that an average of 125 kt of N yr^{-1} was reduced in groundwater at the national scale. At the catchment scale, higher groundwater N reduction was observed in western Jutland, particularly in the southeast, with values up to 86 kg N ha^{-1} yr^{-1} (Figure 3a). In contrast, in Zealand, the N reduction in groundwater ranged from 0 to 10 kg N ha^{-1} yr^{-1} (Figure 3a). These regional variabilities can be attributed to hydrogeological differences. In eastern Jutland and Zealand, drain flow is the main N pathway (Møller et al., 2018), whereas in western Jutland, the sandy soils result in lower drain flow, and N is instead transported via groundwater (Møller et al., 2018). In addition, nitrate leaching in western Jutland is relatively high due to intensive animal farming and high infiltration in the sandy soils. As a result, groundwater's contribution to N reduction at the catchment level becomes more pronounced in western Jutland.

We estimated that DIC production in groundwater by denitrification of nitrate leached from the agricultural soils, for the D5, D10, and D15 models, was 182 (standard deviation (SD): 10.58), 204 (SD: 11.25), and 229 (SD:10.50) kt of CO_2 yr^{-1}, respectively. Like N reduction, CO_2 production exhibited spatial heterogeneity. Western Jutland showed moderately high DIC production, ranging from 60 to 145 kg CO_2 ha^{-1} yr^{-1}. The highest DIC production was predicted in northern Jutland (up to 180 kg CO_2 ha^{-1} yr^{-1}; Figure 3b). In this region, groundwater N reduction was moderate, and organic carbon-mediated denitrification was predicted (Figure 3a). Compared to pyrite oxidation, which releases 0.33 moles of DIC per mole of N reduction, organic matter-mediated denitrification increases 1.25 moles of DIC per mole of N reduction (Table 1). Consequently, more DIC, thus more CO_2, is produced by denitrification in this region.

https://doi.org/10.5194/egusphere-2024-3706
Preprint. Discussion started: 9 December 2024

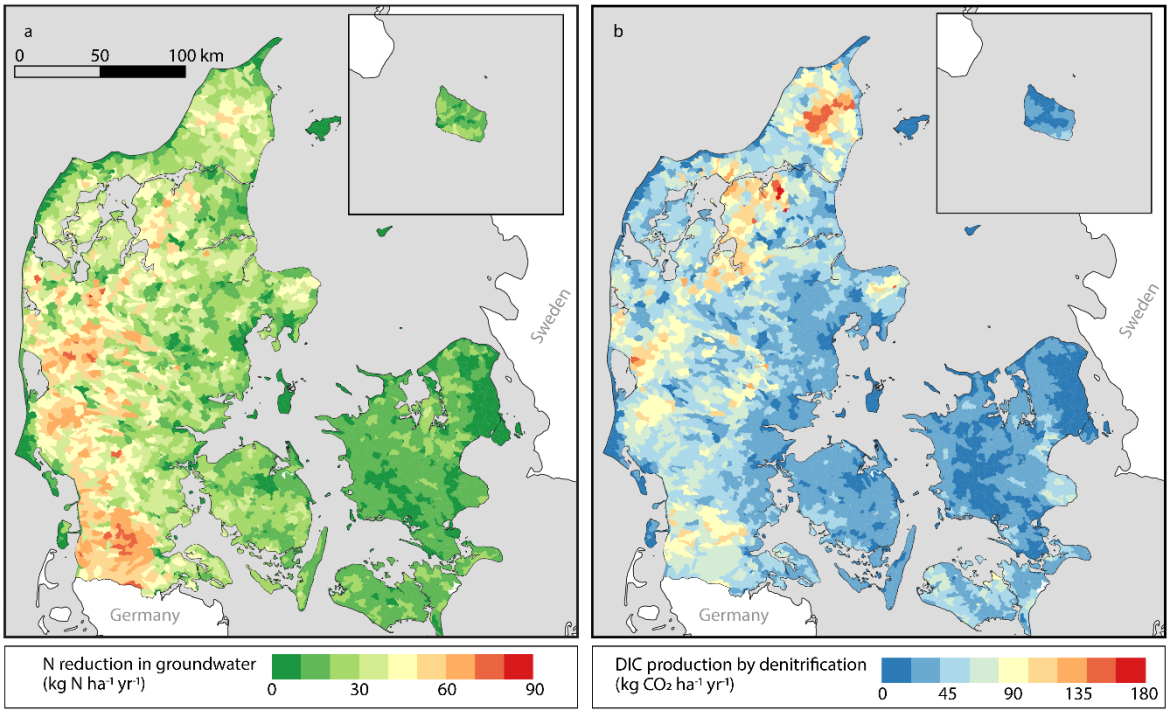

Figure 3. Maps of estimates of (a) nitrate reduction in groundwater in kg N ha^{-1} yr^{-1} and (b) DIC production by denitrification at the catchment scale in kg CO_2 ha^{-1} yr^{-1}.

3.4. Contribution of denitrification in the national inventory of greenhouse gas emissions

Agriculture in Denmark is the second-largest contributor to greenhouse gas emissions excluding land use, land-use change and forestry (LULUCF; Nielsen et al., 2022). According to the IPCC guidelines, the current national inventory for the agriculture sector includes emissions from 1) CH_4 due to enteric fermentation, manure management, and field burning; 2) N_2O from manure management, N-fertilizer use in agricultural soils and field burning; and 3) CO_2 from liming, urea, and other C-containing fertilizers (Nielsen et al., 2022). In 2020, the agricultural sector of Denmark emitted a total of 11,268 kt CO_2-eq. yr^{-1} GHGs, primarily as CH_4 (5,881 kt CO_2-eq. yr^{-1}) and N_2O (5,132 kt CO_2-eq. yr^{-1}; Figure 4). Carbon dioxide accounted for about 2 % (254 kt CO_2-eq. yr^{-1}) of the total GHG emissions from agriculture (Figure 4). The largest source of CO_2 was liming (250 kt of CO_2-eq. yr^{-1}), followed by other C-containing fertilizers (4 kt of CO_2-eq. yr^{-1}) and urea (1 kt of CO_2-eq. yr^{-1}).

https://doi.org/10.5194/egusphere-2024-3706
Preprint. Discussion started: 9 December 2024

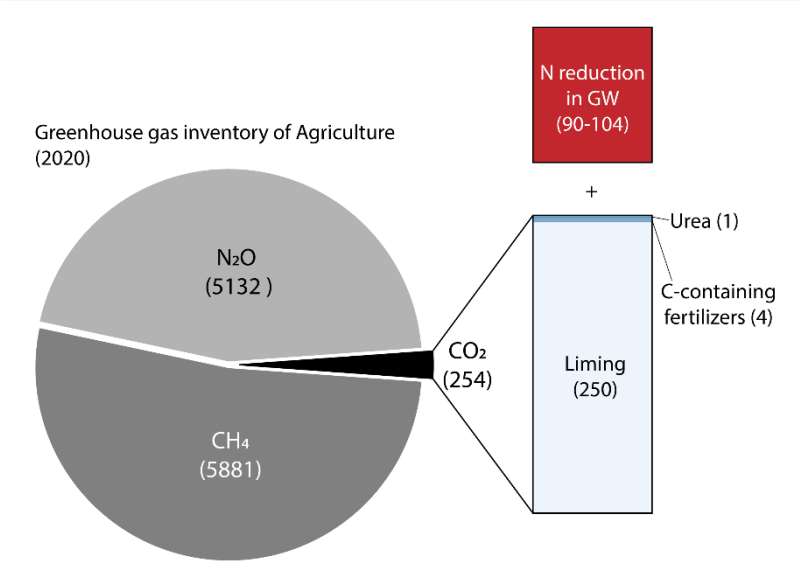

Figure 4. National inventory of greenhouse gas emissions from Danish agriculture. The numbers represent GHG emissions in kt of CO_2 equivalent yr^{-1}. The red box labeled "N reduction in GW" shows the potential CO_2 emissions from denitrification in groundwater estimated in this study.

Our study estimated that approximately 204 kt of CO_2-eq. yr^{-1} of DIC is produced by denitrification in groundwater. The actual magnitude of CO_2 emissions from groundwater depends on various physicochemical conditions, particularly the degree of calcite saturation of groundwater as CO_2 degasses. Among the groundwater screens used for the D10 prediction, 476 of them had field measured pH values. Calculated using PHREEQC (Parkhurst and Appelo, 2013), their log(pCO_2) levels ranged between -2.14 (7,244 µatm) to -1.49 (32,359 µatm; Figure 5a), and saturation indices (SI) for calcite (SI_{CaCO3}) were close to zero except for cluster 7 (-3.72; Figure 5b). Assuming equilibration with atmospheric pCO_2 (400 µatm), the SI_{CaCO3} of these groundwater screens would increase by approximately 1-2 order of magnitude (Figure 5c). These results suggest (based on Table 1) that for cluster 1, 3, 4, 6, and 8, approximately half of the DIC produced by denitrification will be emitted into the atmosphere with the remainder being re-stored as calcite. We further quantified the distribution of the increased DIC between CO_2 emissions, calcite precipitation and the solution using PHREEQC by taking cluster 2 (oxic cluster) as initial conditions (Supplementary Text s1). PHREEQC results indicated that half of the increased DIC was emitted as CO_2, while the remainder was precipitated as calcite (30 to 66% of the increased DIC) or stayed in solution as bicarbonate (-15 to 10% of the increased DIC).

https://doi.org/10.5194/egusphere-2024-3706
Preprint. Discussion started: 9 December 2024

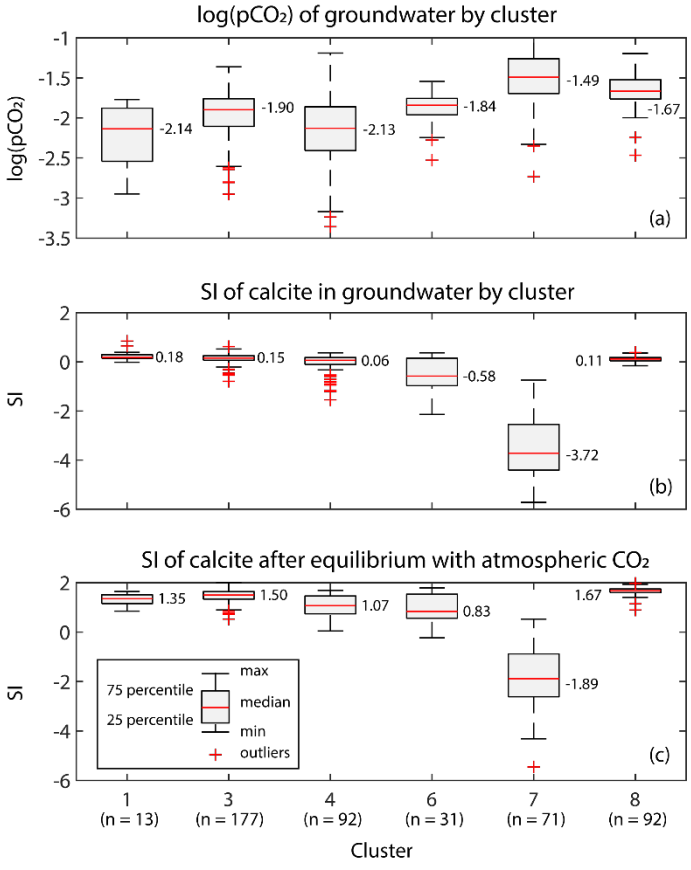

Figure 5. Box plots of (a) log of pCO_2 of groundwater by cluster, (b) saturation index (SI) of calcite in groundwater by cluster, (c) SI of calcite in groundwater after equilibrium with atmospheric CO_2 by cluster.

370

In cluster 7, however, carbonate may have originated primarily from liming, meaning its CO_2 emissions were already accounted as liming; thus, no CO_2 will be emitted due to denitrification. On the other hand, cluster 7 groundwater could pass through the carbonate front, becoming saturated with calcite before discharging into the stream. In this case, its ratio of CO_2 emission per N reduction will be the same as cluster 3. Taking these two cases as the minimum and maximum limits, we 375 estimated that 90-104 kt of CO_2 yr^{-1} will be emitted due to denitrification in groundwater. It is important to note that CO_2 production from denitrification in streams and estuaries was not included in this estimation. For comparison, Martinsen et al. (2024), using machine learning models with observational data and hydrological model outputs, estimated that about 513 kt of CO_2 yr^{-1} is released from the national stream network (Martinsen et al., 2024), and the specific effect of nitrate in this is not given.

380 We conclude that denitrification in groundwater is an important source of anthropogenic CO_2, comparable to liming and up to two orders of magnitude larger than other CO_2 sources currently listed in the IPCC guidelines. Our findings, hence, suggest that current estimations of CO_2 emissions from the agricultural sector are underestimated by at least 35%. These

https://doi.org/10.5194/egusphere-2024-3706
Preprint. Discussion started: 9 December 2024

results clearly demonstrate the need for the IPCC guidelines for greenhouse gas inventories to include CO_2 emissions from denitrification.

Nitrate pollution is a major environmental issue around the world. Research and policy efforts have primarily focused on water quality impact, such as eutrophication and public health concerns. However, our study underscores the need to pay greater attention to the climatic consequences of nitrate pollution as well as N fertilizer use and management. Remediation and restoration efforts for nitrate pollution will inevitably lead to anthropogenic CO_2 emissions. Thus, more holistic approaches are necessary to address both water quality and climate impact.

4. Conclusion

In this study, we evaluated the role of groundwater denitrification of nitrate from agricultural N use as a significant anthropogenic net source of CO_2 from agriculture at the national scale. Using the long-term dataset of groundwater chemistry, we characterized the subsurface redox architecture and identified the dominant denitrification processes. This point-scale information was then scaled up to the national level to produce a predictive map of denitrification processes at the redox interface. The denitrification map highlighted the critical role of hydrogeology in shaping dominance processes by controlling the availability of inorganic carbon and types of reduced materials i.e., pyrite and organic carbon. By integrating these findings with the NKM estimates of N reduction in groundwater, we calculated that denitrification contributed about 205kt of CO_2 as DIC in groundwater annually, with about half of this CO_2 likely released into the atmosphere when groundwater discharges into surface waters.

Our results revealed that in Denmark CO_2 emissions from groundwater denitrification are comparable to those from liming, a predominant source of CO_2 in the agricultural sector. To our best knowledge, this is the first study to quantify the contribution of groundwater denitrification to atmospheric CO_2. Other than liming, the current IPCC guidelines on greenhouse gas inventory account CO_2 emissions from urea and C-containing fertilizers, which are up to two orders of magnitude smaller than those from denitrification in groundwater in Denmark. This suggests that the current CO_2 emissions from the agriculture sector are underestimating total emissions by approximately 38%. Our findings emphasize the urgent need to include CO_2 emissions from groundwater in agricultural GHG inventories.

Denitrification is a natural process and is necessary for mitigate nitrate pollution in groundwater. However, it inevitably releases CO_2 through the mineralizing organic C or carbonate minerals. These geological C sources would otherwise remain stably over geological timescales. Restoring these losses will be challenging. Therefore, strategies addressing N pollution in aquatic ecosystems, particularly in groundwater, must consider both water quality management and climate impact comprehensively.

https://doi.org/10.5194/egusphere-2024-3706
Preprint. Discussion started: 9 December 2024

Data availability

All groundwater chemistry data is available on the National Borehole Database (www.geus.dk/jupiter). The data for predicting the national map is available under following DOI: 10.22008/FK2/I9YCF6 (Koch, 2004).

Author contribution

HK, JK, BGH, and RJ contributed to conceptualization. HK and JK conducted analyses. HK acquired funding and managed the project. HK wrote the original draft and revised it with comments from all coauthors.

Acknowledgements

This project was funded by Geocenter, Denmark. We thank Anker Lajer Højberg for providing the results of NKM.

Financial support

This project was funded by Geocenter, Denmark: Emission of geologic C by agricultural nitrate leaching – an overlooked CO_2 source in terrestrial ecosystems? (2021)

Competing interests

The authors declare that they have no conflict of interest.

https://doi.org/10.5194/egusphere-2024-3706
Preprint. Discussion started: 9 December 2024

References

Adhikari, K., Kheir, R. B., Greve, M. B., Bøcher, P. K., Malone, B. P., Minasny, B., McBratney, A. B., and Greve, M. H.: High-Resolution 3-D Mapping of Soil Texture in Denmark, Soil Sci. Soc. Am. J., 77, 860–876, https://doi.org/10.2136/sssaj2012.0275, 2013.

Adhikari, K., Hartemink, A. E., Minasny, B., Bou Kheir, R., Greve, M. B., and Greve, M. H.: Digital Mapping of Soil Organic Carbon Contents and Stocks in Denmark, PLoS One, 9, e105519, https://doi.org/10.1371/journal.pone.0105519, 2014.

Appelo, C. A. J. and Postma, D.: Geochemistry, Groundwater and Pollution, edited by: Appelo, C. A. J. and Postma, D., CRC Press, https://doi.org/10.1201/9781439833544, 2005.

Ascott, M. J., Gooddy, D. C., Wang, L., Stuart, M. E., Lewis, M. A., Ward, R. S., and Binley, A. M.: Global patterns of nitrate storage in the vadose zone, Nat. Commun., 8, 1–6, https://doi.org/10.1038/s41467-017-01321-w, 2017.

Barak, P., Jobe, B. O., Krueger, A. R., Peterson, L. A., and Laird, D. A.: Effects of long-term soil acidification due to nitrogen fertilizer inputs in Wisconsin, Plant Soil, 197, 61–69, https://doi.org/10.1023/A:1004297607070, 1997.

Basu, N. B., Van Meter, K. J., Byrnes, D. K., Van Cappellen, P., Brouwer, R., Jacobsen, B. H., Jarsjö, J., Rudolph, D. L., Cunha, M. C., Nelson, N., Bhattacharya, R., Destouni, G., and Olsen, S. B.: Managing nitrogen legacies to accelerate water quality improvement, Nat. Geosci., 15, 97–105, https://doi.org/10.1038/s41561-021-00889-9, 2022.

Bjerager, M. and Surlyk, F.: Benthic palaeoecology of Danian deep-shelf bryozoan mounds in the Danish Basin, Palaeogeogr. Palaeoclimatol. Palaeoecol., 250, 184–215, https://doi.org/10.1016/j.palaeo.2007.03.008, 2007.

Børgesen, C. D., Sørensen, P., Blichers-Mathiesen, G., Kristensen, K. M., Pullens, J. W. M., Zhao, J., and Olesen, J. E.: NLES5 - An empirical model for prediciting nitrate leaching from the root zone of agricultural land in Denmark, 116 pp., 2020.

Damholt, S. F., Bjerager, M., and Damholt, T.: Stevns Klint, Denmark: Uppermost Maastrichtian chalk, Cretaceous–Tertiary boundary, and lower Danian bryozoan mound complex, Bull. Geol. Soc. Denmark, 54, 1–48, https://doi.org/10.37570/bgsd-2006-54-01, 2006.

Diaz, R. J. and Rosenberg, R.: Spreading Dead Zones and Consequences for Marine Ecosystems, Science (80-.)., 321, 926–929, https://doi.org/10.1126/science.1156401, 2008.

Duvert, C., Butman, D. E., Marx, A., Ribolzi, O., and Hutley, L. B.: CO2 evasion along streams driven by groundwater inputs and geomorphic controls, Nat. Geosci., 11, 813–818, https://doi.org/10.1038/s41561-018-0245-y, 2018.

Galloway, J. N., Aber, J. D., Erisman, J. W., Seitzinger, S. P., Howarth, R. W., Cowling, E. B., Cosby, B. J., and Galloway,, J. N.: The Nitrogen Cascade, Bioscience, 53, 341–356, https://doi.org/https://doi.org/10.1641/0006-3568(2003)053[0341:TNC]2.0.CO;2, 2003.

Gao, Y. and Cabrera Serrenho, A.: Greenhouse gas emissions from nitrogen fertilizers could be reduced by up to one-fifth of current levels by 2050 with combined interventions, Nat. Food, 4, 170–178, https://doi.org/10.1038/s43016-023-00698-w,

2023.

Haggerty, R., Sun, J., Yu, H., and Li, Y.: Application of machine learning in groundwater quality modeling - A comprehensive review, Water Res., 233, 119745, https://doi.org/10.1016/j.watres.2023.119745, 2023.

Hansen, L. K., Jakobsen, R., and Postma, D.: Methagnogenesis in a shallow sandy aquifer, Rømø, Denmark, Geochim. Cosmochim. Acta, 65, 2925–2935, https://doi.org/10.1016/S0016-7037(01)00653-6, 2001.

Henriksen, H. J., Troldborg, L., Nyegaard, P., Sonnenborg, T. O., Refsgaard, J. C., and Madsen, B.: Methodology for construction, calibration and validation of a national hydrological model for Denmark, J. Hydrol., 280, 52–71, https://doi.org/10.1016/S0022-1694(03)00186-0, 2003.

Højberg, A., Troldborg, L., Tornbjerg, H., Windolf, J., Blicher-Mathiesen, G., Thodsen, H., Kronvang, B., and Børgesen, C.: Development of a Danish national nitrogen model – input to a new spatial differentiated regulation, LuWQ2015, L. Use Water Qual. Agric. Prod. Environ. Vienna, Austria, 21-24 Sept. 2015, 2015.

Højberg, A. L., Hansen, A. L., Wachniew, P., Żurek, A. J., Virtanen, S., Arustiene, J., Strömqvist, J., Rankinen, K., and Refsgaard, J. C.: Review and assessment of nitrate reduction in groundwater in the Baltic Sea Basin, J. Hydrol. Reg. Stud., 12, 50–68, https://doi.org/10.1016/j.ejrh.2017.04.001, 2017.

Højberg, A. L., Thodsen, H., Duus Børgesen, C., Tornbjerg, H., Nordstrøm, B. O., Troldborg, L., Christian Hoffmann, C., Kjeldgaard, A., Holm, H., Audet, J., Ellermann, T., Heile Christensen, J., Bach, E. O., and Pedersen, B. F.: National kvælstofmodel – version 2020. Opdatering af nationalt retentionskort. Metode rapport, 2021.

Howarth, R., Chan, F., Conley, D. J., Garnier, J., Doney, S. C., Marino, R., and Billen, G.: Coupled biogeochemical cycles: Eutrophication and hypoxia in temperate estuaries and coastal marine ecosystems, Front. Ecol. Environ., 9, 18–26, https://doi.org/10.1890/100008, 2011.

IPCC: 2006 IPCC Guidelines for National Greenhouse Gas Inventories, Prepared by the National Greenhouse Gas Inventories Programme, Eggleston H.S., Buendia L., Miwa K., Ngara T. and Tanabe K. (eds). Published: IGES, Japan., 2006.

Jakobsen, R. and Cold, L.: Geochemistry at the sulfate reduction-methanogenesis transition zone in an anoxic aquifer-A partial equilibrium interpretation using 2D reactive transport modeling, Geochim. Cosmochim. Acta, 71, 1949–1966, https://doi.org/10.1016/j.gca.2007.01.013, 2007.

Jakobsen, R. and Postma, D.: Redox zoning, rates of sulfate reduction and interactions with Fe-reduction and methanogenesis in a shallow sandy aquifer, Romo, Denmark, Geochim. Cosmochim. Acta, 63, 137–151, https://doi.org/10.1016/S0016-7037(98)00272-5, 1999.

Jensen, A. S., Coffman, V. R., Schullehner, J., Trabjerg, B. B., Pedersen, C. B., Hansen, B., Olsen, J., Pedersen, M., Stayner, L. T., and Sigsgaard, T.: Prenatal exposure to tap water containing nitrate and the risk of small-for-gestational-age: A nationwide register-based study of Danish births, 1991–2015, Environ. Int., 174, 107883, https://doi.org/10.1016/j.envint.2023.107883, 2023.

Jessen, S., Postma, D., Thorling, L., Müller, S., Leskelä, J., and Engesgaard, P.: Decadal variations in groundwater quality:

https://doi.org/10.5194/egusphere-2024-3706
Preprint. Discussion started: 9 December 2024

A legacy from nitrate leaching and denitrification by pyrite in a sandy aquifer, Water Resour. Res., 53, 184–198, https://doi.org/10.1002/2016WR018995, 2017.

Jorgensen, N. O.: Dolomite and dedolomitization in Danian bryozoan limestone from Fakse, Denmark, Bull. - Geol. Soc. Denmark, 37, 63–74, https://doi.org/10.37570/bgsd-1988-37-06, 1988.

Kaiser, K., Rother, H., Lorenz, S., Gärtner, P., and Papenroth, R.: Geomorphic evolution of small river–lake-systems in northeast Germany during the Late Quaternary, Earth Surf. Process. Landforms, 32, 1516–1532, https://doi.org/10.1002/esp.1480, 2007.

Ke, G., Meng, Q., Finley, T., Wang, T., Chen, W., Ma, W., Ye1, Q., and Liu, T.-Y.: LightGBM: A Highly Efficient Gradient Boosting Decision Tree, in: 31st Conference on Neural Information Processing Systems (NIPS 2017), 2017.

Kim, H., Sandersen, P. B. E., Jakobsen, R., Kallesøe, A. J., Claes, N., Blicher-Mathiesen, G., Foged, N., Aamand, J., and Hansen, B.: A 3D hydrogeochemistry model of nitrate transport and fate in a glacial sediment catchment: A first step toward a numerical model, Sci. Total Environ., 776, 146041, https://doi.org/10.1016/j.scitotenv.2021.146041, 2021.

Koch, J.: Groundwater Redox Modeling Denmark, GEUS Dataverse, https://doi.org/10.22008/FK2/I9YCF6, 2004.

Koch, J., Kim, H., Tirado-Conde, J., Hansen, B., Møller, I., Thorling, L., Troldborg, L., Voutchkova, D., and Højberg, A. L.: Modeling groundwater redox conditions at national scale through integration of sediment color and water chemistry in a machine learning framework, Sci. Total Environ., 947, 174533, https://doi.org/10.1016/j.scitotenv.2024.174533, 2024.

Liu, J., You, L., Amini, M., Obersteiner, M., Herrero, M., Zehnder, A. J. B., and Yang, H.: A high-resolution assessment on global nitrogen flows in cropland, Proc. Natl. Acad. Sci. U. S. A., 107, 8035–8040, https://doi.org/10.1073/pnas.0913658107, 2010.

Lundberg, S. M. and Lee, S. I.: A unified approach to interpreting model predictions, Adv. Neural Inf. Process. Syst., 2017-Decem, 4766–4775, 2017.

Macpherson, G. L. L.: CO2 distribution in groundwater and the impact of groundwater extraction on the global C cycle, Chem. Geol., 264, 328–336, https://doi.org/10.1016/j.chemgeo.2009.03.018, 2009.

Martinsen, K. T., Sand-Jensen, K., Bergmann, V., Skjærlund, T., Kjær, J. E., and Koch, J.: Seasonal Carbon Dioxide Concentrations and Fluxes Throughout Denmark's Stream Network, J. Geophys. Res. Biogeosciences, 129, https://doi.org/10.1029/2024JG008031, 2024.

Meals, D. W., Dressing, S. A., and Davenport, T. E.: Lag Time in Water Quality Response to Best Management Practices: A Review, J. Environ. Qual., 39, 85–96, https://doi.org/10.2134/jeq2009.0108, 2010.

Menegat, S., Ledo, A., and Tirado, R.: Greenhouse gas emissions from global production and use of nitrogen synthetic fertilisers in agriculture, Sci. Rep., 12, 1–13, https://doi.org/10.1038/s41598-022-18773-w, 2022.

Møller, A. B., Beucher, A., Iversen, B. V., and Greve, M. H.: Predicting artificially drained areas by means of a selective model ensemble, Geoderma, 320, 30–42, https://doi.org/10.1016/j.geoderma.2018.01.018, 2018.

Mosier, A., Kroeze, C., Nevison, C., Oenema, O., and Seitzinger, S.: Closing the global N2O budget: nitrous oxide emissions through the agricultural nitrogen cycle, Nutr. Cycl. Agroecosystems, 52, 225–248,

https://doi.org/10.1023/A:1009740530221, 1998.

Nielsen, O., Winther, M., Nielsen, M., Gyldenkærne, S., and Thomsen, M.: Denmark ' S National Inventory Report 2022: Emission Inventories 1990-2020 – Submitted under the United Nations Framework Convention on Climate Change and the Kyoto Protocol, 947 pp., 2022.

Parkhurst, D. L. and Appelo, C. A. J.: Description of input and examples for PHREEQC version 3: a computer program for speciation, batch-reaction, one-dimensional transport, and inverse geochemical calculations, https://doi.org/10.3133/tm6A43, 2013.

Perrin, A.-S., Probst, A., and Probst, J.-L.: Impact of nitrogenous fertilizers on carbonate dissolution in small agricultural catchments: Implications for weathering CO2 uptake at regional and global scales, Geochim. Cosmochim. Acta, 72, 3105–3123, https://doi.org/10.1016/j.gca.2008.04.011, 2008.

Postma, D., Boesen, C., Kristiansen, H., and Larsen, F.: Nitrate Reduction in an Unconfined Sandy Aquifer: Water Chemistry, Reduction Processes, and Geochemical Modeling, Water Resour. Res., 27, 2027–2045, https://doi.org/10.1029/91WR00989, 1991.

Postma, D., Larsen, F., Thai, N. T., Trang, P. T. K., Jakobsen, R., Nhan, P. Q., Long, T. V., Viet, P. H., and Murray, A. S.: Groundwater arsenic concentrations in Vietnam controlled by sediment age, Nat. Geosci., 5, 656–661, https://doi.org/10.1038/ngeo1540, 2012.

Ritchie, H., Rosado, P., and Roser, M.: "Breakdown of carbon dioxide, methane and nitrous oxide emissions by sector" Published online at OurWorldinData.org. Retrieved from: "https://ourworldindata.org/emissions-by-sector" [Online Resource], 2023.

Sandersen, P.: A basic geological complexity map for use in the implementation of the MapField concept, 2021.

Schullehner, J., Hansen, B., Thygesen, M., Pedersen, C. B., and Sigsgaard, T.: Nitrate in drinking water and colorectal cancer risk: A nationwide population-based cohort study, Int. J. Cancer, 143, 73–79, https://doi.org/10.1002/ijc.31306, 2018.

Seitzinger, S., Harrison, J. A., Böhlke, J. K., Bouwman, A. F., Lowrance, R., Peterson, B., Tobias, C., and Van Drecht, G.: Denitrification across landscapes and waterscapes: A synthesis, Ecol. Appl., 16, 2064–2090, https://doi.org/10.1890/1051-0761(2006)016[2064:DALAWA]2.0.CO;2, 2006.

Shaughnessy, A. R., Gu, X., Wen, T., and Brantley, S. L.: Machine learning deciphers CO2 sequestration and subsurface flowpaths from stream chemistry, Hydrol. Earth Syst. Sci., 25, 3397–3409, https://doi.org/10.5194/hess-25-3397-2021, 2021.

Stets, E. G., Kelly, V. J., and Crawford, C. G.: Long-term trends in alkalinity in large rivers of the conterminous US in relation to acidification, agriculture, and hydrologic modification, Sci. Total Environ., 488–489, 280–289, https://doi.org/10.1016/j.scitotenv.2014.04.054, 2014.

Stisen, S., Ondracek, M., Troldborg, L., Schneider, R. J. M., and van Til, M. J.: National Vandressource Model - Modelopstilling og kalibrering af DK-model 2019, https://doi.org/10.22008/gpub/32631, 2019.

Syakur, M. A., Khotimah, B. K., Rochman, E. M. S., and Satoto, B. D.: Integration K-Means Clustering Method and Elbow Method for Identification of the Best Customer Profile Cluster, IOP Conf. Ser. Mater. Sci. Eng., 336,

https://doi.org/10.5194/egusphere-2024-3706
Preprint. Discussion started: 9 December 2024

https://doi.org/10.1088/1757-899X/336/1/012017, 2018.

Temkin, A., Evans, S., Manidis, T., Campbell, C., and Naidenko, O. V.: Exposure-based assessment and economic valuation of adverse birth outcomes and cancer risk due to nitrate in United States drinking water., Environ. Res., 176, 108442, https://doi.org/10.1016/j.envres.2019.04.009, 2019.

Thorling, L., Albers, C. N., Ditlefsen, D., Hansen, B., Johnsen, A. R., Kazmierczak, J., Mortensen, M. H., and Troldborg, L.: Grundvand. Status og udvikling 1989–2022, 1–147 pp., 2024.

Torrentó, C., Cama, J., Urmeneta, J., Otero, N., and Soler, A.: Denitrification of groundwater with pyrite and Thiobacillus denitrificans, Chem. Geol., 278, 80–91, https://doi.org/10.1016/j.chemgeo.2010.09.003, 2010.

Trends, R., Galloway, J. N., Townsend, A. R., Erisman, J. W., Bekunda, M., Cai, Z., Freney, J. R., Martinelli, L. a, Seitzinger, S. P., and Sutton, M. a: Transformation of the Nitrogen Cycle, Science (80-.)., 320, 889–892, 2008.

Vesselinov, V. V., Alexandrov, B. S., and O'Malley, D.: Contaminant source identification using semi-supervised machine learning, J. Contam. Hydrol., 212, 134–142, https://doi.org/10.1016/j.jconhyd.2017.11.002, 2018.

Ward, M., Jones, R., Brender, J., de Kok, T., Weyer, P., Nolan, B., Villanueva, C., and van Breda, S.: Drinking Water Nitrate and Human Health: An Updated Review, Int. J. Environ. Res. Public Health, 15, 1557, https://doi.org/10.3390/ijerph15071557, 2018.

Zamanian, K., Zarebanadkouki, M., and Kuzyakov, Y.: Nitrogen fertilization raises CO2 efflux from inorganic carbon: A global assessment, Glob. Chang. Biol., 24, 2810–2817, https://doi.org/10.1111/gcb.14148, 2018.

Zhang, Y. C., Slomp, C. P., Broers, H. P., Passier, H. F., and Cappellen, P. Van: Denitrification coupled to pyrite oxidation and changes in groundwater quality in a shallow sandy aquifer, Geochim. Cosmochim. Acta, 73, 6716–6726, https://doi.org/10.1016/j.gca.2009.08.026, 2009.